

LETTER • OPEN ACCESS

Intensity-duration-frequency curves at the global scale

To cite this article: Laurent G Courty *et al* 2019 *Environ. Res. Lett.* **14** 084045

View the [article online](#) for updates and enhancements.



LETTER

Intensity-duration-frequency curves at the global scale

OPEN ACCESS

RECEIVED
1 April 2019

REVISED
29 July 2019

ACCEPTED FOR PUBLICATION
30 July 2019

PUBLISHED
14 August 2019

Laurent G Courty^{1,2} , Robert L Wilby¹ , John K Hillier¹ and Louise J Slater³

¹ Department of Geography and Environment, Loughborough University, LE11 3TU, United Kingdom

² Mexican Institute of Water Technology, 62550 Jiutepec, Morelos, Mexico

³ School of Geography and Environment, University of Oxford, OX1 3QY, United Kingdom

E-mail: laurent_courty@tlaloc.imta.mx

Keywords: frequency analysis, precipitation, design rainfall, ERA5, reanalysis

Supplementary material for this article is available [online](#)

Original content from this work may be used under the terms of the [Creative Commons Attribution 3.0 licence](#).

Any further distribution of this work must maintain attribution to the author(s) and the title of the work, journal citation and DOI.

**Abstract**

Intensity-duration-frequency (IDF) curves usefully quantify extreme precipitation over various durations and return periods for engineering design. Unfortunately, sparse, infrequent, or short observations hinder the creation of robust IDF curves in many locations. This paper presents the first global, multi-temporal (1–360 h) dataset of generalized extreme value (GEV) parameters at 31 km resolution dubbed PXR-2 (Parametrized eXtreme Rain). Using these data we generalize site-specific studies to show that that GEV parameters typically scale robustly with event duration ($r^2 > 0.88$). Thus, we propose a universal IDF formula that allows estimates of rainfall intensity for a continuous range of durations (PXR-4). This parameter scaling property opens the door to estimating sub-daily IDF from daily records. We evaluate this characteristic for selected global cities and a high-density rain gauge network in the United Kingdom. We find that intensities estimated with PXR-4 are within $\pm 20\%$ of PXR-2 for durations ranging between 2 and 360 h. PXR is immediately usable by earth scientists studying global precipitation extremes and a promising proof-of-concept for engineers designing infrastructure in data-scarce regions.

1. Introduction

Historical precipitation records are widely employed by civil engineers to compute intensity-duration-frequency (IDF) curves, which are essential for the design of infrastructure like highways (e.g. Brown *et al* 2013, NYS DoT 2018), urban drainage networks (e.g. Battaglia *et al* 2003, Brown *et al* 2013) and dams (e.g. NYS DoEC 1989). Indeed, IDF curves are used to create synthetic rainfalls that permit the sizing of structures for a given return period, often required by local regulations.

However, not all countries have historical rain gauge records that are long or dense enough to compute reliable IDF curves (e.g. Lumbroso *et al* 2011). The lack of observational data for IDF analysis is particularly true in continents such as Africa (van de Giesen *et al* 2014) and Asia, where most of the world's urbanization is expected to take place over coming decades (UN DESA 2018). As a result, much new infrastructure is being built in regions where the historical record of

precipitation is scarce or uncertain, hindering adequate sizing of water-related works.

The first limitation of the observational data records is the scarcity of spatial coverage. The classical solution to this problem is to interpolate rainfall between weather stations. However, interpolation performs poorly in locations where pluviometers are sparse (e.g. Xu *et al* 2015, Kumari *et al* 2017). A more sophisticated approach consists of analyzing regional precipitation patterns to estimate local characteristics such as IDF curves at the location of interest (e.g. Roux and Desbordes 1996, Fowler and Kilsby 2003, Domínguez *et al* 2018). Most recently, IDF curves have been derived over the continental US (Ombadi *et al* 2018) using the PERSIANN-CDR satellite-based precipitation dataset (Ashouri *et al* 2015). However, a global, consistent IDF dataset is still lacking.

The increasing resolution and reliability of global or near-global gridded precipitation datasets represents a key opportunity to develop alternative approaches to tackle engineering challenges such as the

correct sizing of flood infrastructure. Global gridded precipitation estimates are typically obtained by meteorological reanalysis (e.g. Uppala *et al* 2005, Gelaro *et al* 2017) where weather observations are assimilated by numerical weather prediction models to estimate precipitation. Advanced data fusion schemes have been developed by merging gauge-, satellite-, and reanalysis-based data to generate enhanced global precipitation estimates (e.g. Beck *et al* 2018, Sun *et al* 2018). Although global weather data products are widely employed by the Earth science community, their use in engineering is still limited to applications such as wind power generation (e.g. Staffell and Pfenninger 2016, Olauson 2018) or drought monitoring (e.g. Hao *et al* 2014). This paper is the first attempt to study global IDF relationships using gridded precipitation datasets, in an effort to help address the issue of precipitation data scarcity.

A second issue that is common with precipitation data is that of temporal resolution. In many cases, sub-daily IDF records are required for engineering uses because small catchments that are sensitive to brief rainfall events often require appropriate storm-water drainage structures. There have been recent efforts to compile high-resolution rainfall datasets (Blenkinsop *et al* 2018), however the vast majority of historical precipitation data are still collected at a daily resolution in most parts of the world. Such low temporal resolution presents a major challenge for engineers designing urban water infrastructure, where catchments are commonly tens of hectares with lag times of less than an hour (Berne *et al* 2004).

This temporal limitation might be overcome by using a duration scaling property of IDF curves to estimate sub-daily IDF from daily precipitation. Extreme precipitation intensities for a given event duration d typically follow a generalized extreme value (GEV) distribution, and it has been shown that the location and scale parameters of the GEV scale with d (e.g. Menabde *et al* 1999, Veneziano and Furcolo 2002, Bougadis and Adamows 2006, Overeem *et al* 2008). For instance, it has been demonstrated that the IDF characteristic of a given site could be described by a Gumbel distribution where the parameters follow a power law for durations between 30 min and 24 h (Menabde *et al* 1999). However, those studies analyzed only a few sites: 2 in South Africa and Australia (Menabde *et al* 1999), 5 in Canada (Bougadis and Adamows 2006), and 12 in the Netherlands (Overeem *et al* 2008). Therefore it has not been possible to determine whether this scaling property holds at a global scale. This would be of practical interest in many parts of the world where daily rainfall data are more widely available than sub-daily records.

This paper first uses the ERA5 reanalysis to generate global IDF relationships modeled with a GEV distribution, then investigates the extent to which these relationships scale with the event duration d at a global level. The analysis led to the creation of two

datasets. The Parametrized eXtreme Rain-2 (PXR-2) dataset compiles the GEV parameters for 19 event durations spanning 1–360 h, whereas the Parametrized eXtreme Rain-4 (PXR-4) represents the global distribution of the four parameters of a generalized IDF formula.

2. Methodology

2.1. Input data

Precipitation data were obtained from the ERA5 deterministic reanalysis (Hersbach and Dick 2016, Copernicus Climate Change Service 2018) at a spatial resolution of 0.25° (~ 31 km) and temporal resolution of 1 h. We chose the ERA5 dataset for its high spatial and temporal resolution, its performance (Beck *et al* 2018), and its permissive usage license. We employ all the complete calendar years available at the time of writing (i.e. 1979–2018).

We use hourly rain gauge records from the MIDAS database of the UK Meteorological Office (Met Office 2012) as a reference dataset for comparison with the reanalysis data. The original dataset contains 650 stations with variable record lengths. We use only the stations where geographical coordinates are provided. Following Blenkinsop *et al* (2017), we keep only the observations that do not exceed by more than 20% the 1h and 24 h precipitation historical maxima for the UK, defined respectively as 92 mm and 279 mm by Met Office (2018). After this quality control, we omit the years with $<90\%$ of observations remaining, and retain only those stations with $\geq 90\%$ of years remaining over the entire time period. This results in a subset of 35 stations for analysis (see figure S6 available online at stacks.iop.org/ERL/14/084045/mmedia for their location).

2.2. Estimation of distribution parameters

The GEV distribution is widely used to represent annual maxima series (AMS) (e.g. Fowler and Kilsby 2003, Overeem *et al* 2008, Papalexiou and Koutsoyiannis 2013) with the cumulative distribution function (CDF):

$$F(I) = \begin{cases} \exp\left[-\left(\frac{I-\mu}{\sigma}\right)^{1/\kappa}\right] & \text{if } \kappa \neq 0 \\ \exp\left[\exp\left(-\frac{I-\mu}{\sigma}\right)\right] & \text{if } \kappa = 0 \end{cases}, \quad (1)$$

where I is the rainfall intensity, μ the location parameter, σ the scale parameter and κ the shape parameter. Parameters μ and σ have the same unit as I , here mm h^{-1} . This formulation of the GEV implies that the distribution is bounded from below, corresponding to the Fréchet distribution, when $\kappa < 0$ (Hosking *et al* 1985, Overeem *et al* 2008); other authors use a formulation of equation (1) that implies the opposite sign of κ (e.g. Papalexiou and Koutsoyiannis 2013, Ragulina and Reitan 2017). When $\kappa = 0$, the GEV is the Gumbel distribution.

The estimation of κ is notoriously difficult due to its sensitivity to record length (Overeem *et al* 2008, Papalexiou and Koutsoyiannis 2013, Ragulina and Reitan 2017). Indeed, it has been demonstrated that for sample sizes less than 50, using a two parameter Gumbel distribution results in a smaller error than the three parameter GEV (Lu and Stedinger 1992). However, using $\kappa = 0$ could considerably underestimate the precipitation intensity, especially for long return periods (Koutsoyiannis 2004a, 2004b). This represents an important safety concern when designing engineering structures like dams.

On the other hand, studies have found that κ tends to -0.114 irrespective of geographical location (Papalexiou and Koutsoyiannis 2013) and event duration d (Overeem *et al* 2008). Considering the difficulty of robustly estimating κ , and that the value tends to -0.114 independently of duration or geographical location, we decide to globally set the GEV shape parameter to $\kappa = -0.114$.

The parameters of location (μ) and scale (σ) are estimated using the probability-weighted moments (PWMs) method (Hosking *et al* 1985). The confidence intervals of the parameter estimates are obtained via bootstrapping with 1000 samples. We assess the goodness of fit of the distribution using the Filliben test (Wilks 2011). This test is based on a Q–Q plot between the AMS and the quantile estimate (mm h^{-1} , see equation (2)). The probability of exceedance of the AMS is estimated with the Cunnane plotting position (Wilks 2011), and the quantile estimate is calculated at the same return period. The Filliben test statistic consists of the Pearson's correlation coefficient r on that Q–Q plot. The critical value for the test is estimated using the formula given by Heo *et al* (2008). If $r \geq r_{\text{crit}}$ the null hypothesis that the AMS follows the GEV distribution cannot be rejected.

After fitting the GEV, intensity for a given probability is estimated by the inverse of the CDF, also called the quantile function:

$$i(d, T) = \mu_d + \sigma_d y, \quad (2)$$

where y is expressed relative to the return period T in years with $T = 1/(1 - F)$:

$$y = \{1 - [-\ln(1 - 1/T)]^\kappa\} / \kappa. \quad (3)$$

With $\kappa = -0.114$, the variance of the estimated rainfall intensity i can be obtained with the formula proposed by Lu and Stedinger (1992):

$$\text{Var}(i) = \sigma^2(1.142 + 0.8216y + 1.2546y^2)/n, \quad (4)$$

where n is the length of the AMS in years. The confidence interval of the precipitation intensity I can then be estimated as:

$$I \in i \pm t_{n-2}^* \sqrt{\frac{\text{Var}(i)}{n}}, \quad (5)$$

where t_{n-2}^* is the quantile of the Student's t distribution with $n - 2$ degrees of freedom. For a sample size

of 40 years and a 95% confidence interval, this value is 2.024.

2.3. Scaling of distribution parameters

To assess the scaling of the distribution parameters (μ , σ) relative to the event duration, we find the annual maxima for 19 event durations d by using a rolling mean. Window sizes are chosen to reflect a relatively regular spacing on a logarithmic scale and to present an equal number of durations for sub- and super-daily events. The selected durations are 1, 2, 3, 4, 6, 8, 10, 12, 18, 24, 48, 72, 96, 120, 144, 192, 240, 288 and 360 h. Subsequently, the GEV parameters are estimated for each duration and ERA5 cell. Considering the spatial resolution of 0.25° , the 19 durations and the 1000 samples bootstrap, in total the GEV is fitted 1.97×10^{10} times to the AMS. Global maps of the estimated GEV parameters for each duration are compiled in the PXR-2 dataset (Courty *et al* 2019), alongside their uncertainties.

Following Menabde *et al* (1999), we assume that μ and σ scale with d according to a power law, but where they assert a single scaling gradient for both parameters we allow each to scale independently. This independent scaling of the two parameters appears typical for ERA5 data (figures S4 and S5). The scaling is therefore expressed as

$$\mu_d = ad^\alpha \quad \sigma_d = bd^\beta, \quad (6)$$

where d is the event duration in hours and a and α are the scaling parameters for μ , and b and β those for σ . These power-law relationships are straight lines in logarithmic space. For simplicity and ease of reproducibility (e.g. by practitioners) the scaling parameters are then estimated by Ordinary Least Squares (OLS) regression. Pearson's r^2 is used to test the linear relationship of the studied variables. The PXR-4 dataset (Courty *et al* 2019) comprises the global distribution of these four parameters and their uncertainty.

Substituting μ_d and σ_d into equation (2) with their scaled form from equation (6) we obtain a general IDF formula equation (7) that takes the parameters a , α and b , β specific to a given geographical location.

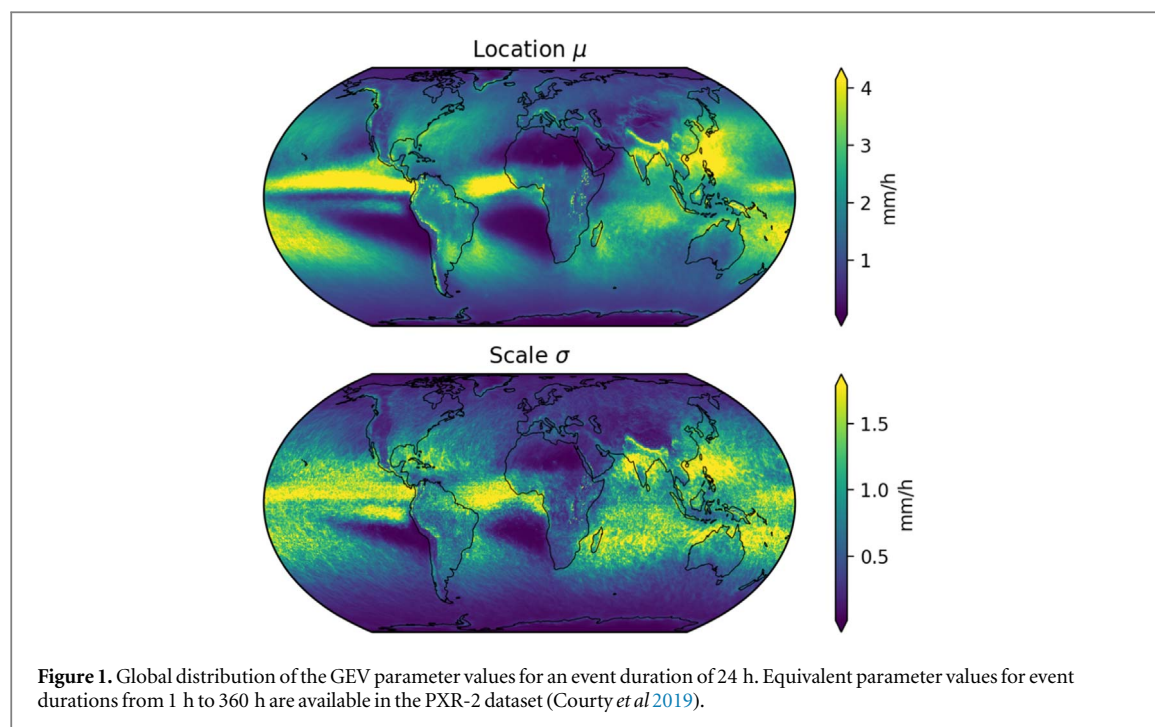
$$i(d, T) = ad^\alpha - bd^\beta y. \quad (7)$$

3. Results

3.1. Global GEV parameters

The PXR-2 dataset comprises worldwide GEV parameters estimated from the ERA5 data for all 19 durations (1–360 h), along with their uncertainties. This set of parameters is made freely available to accompany this paper (Courty *et al* 2019).

The Filliben goodness of fit test indicates that at the 5% significance level the null hypothesis that the annual maxima follow a GEV distribution with $\kappa = -0.114$ can be rejected in 5.7% of the fitted cells



(geographical location and duration). Considering the number of tests involved (19.7×10^6), $\approx 5\%$ of rejection is expected at the 5% significance level (Bland and Altman 1995). Here, the lower goodness of fit occurs in spatially coherent areas, located mostly in the drier regions of the Atlantic and Pacific oceans, the Sahara, the south of the Arabian peninsula, tropical Africa and the upper Amazon (see figure S1). Similar goodness of fit estimates are obtained with the Lilliefors test (see figure S2). The values of the test statistic for goodness of fit are included in the PXR dataset (Courty *et al* 2019).

The GEV parameter maps shown in figure 1 clearly display regional rainfall patterns, such as tropical rainfall and monsoon (e.g. south Asia, Kripalani *et al* 2007), orographic rainfall over mountainous regions (e.g. central Andes, Viale *et al* 2011), and desert areas (e.g. Antarctica, Vaughan *et al* 1999).

3.2. Scaling of the GEV parameters

The fit of the power law relationship between μ or σ and d is quantified by calculating Pearson's r^2 for data presented on a log–log scale. In 99% of the ERA5 cells r^2 exceeds 0.91 for μ and 0.88 for σ . Thus, the GEV parameters (μ , σ) both scale linearly on a log–log scale and this property appears to be robust and consistent at the global scale. The spatial distribution of r^2 values is also more consistent for μ than σ , with greater spatial variability for the latter (see figure S3).

The global distribution of the scaling gradients (α , β) is shown in figure 2. The spatial distribution of α seems to follow patterns with steeper gradients in deserts (e.g. Baja California, Patagonia, Sahara, Namib, Arabian peninsula, Taklamakan, Gobi) and smaller gradients in mountain ranges (e.g. Andes,

Sierra Nevada, East African Rift, Scandes, Alps, Ural, Alborz, Caucasus, Himalaya, Kamchatka). β appears to follow similar patterns, but associated with a greater spatial variability than α .

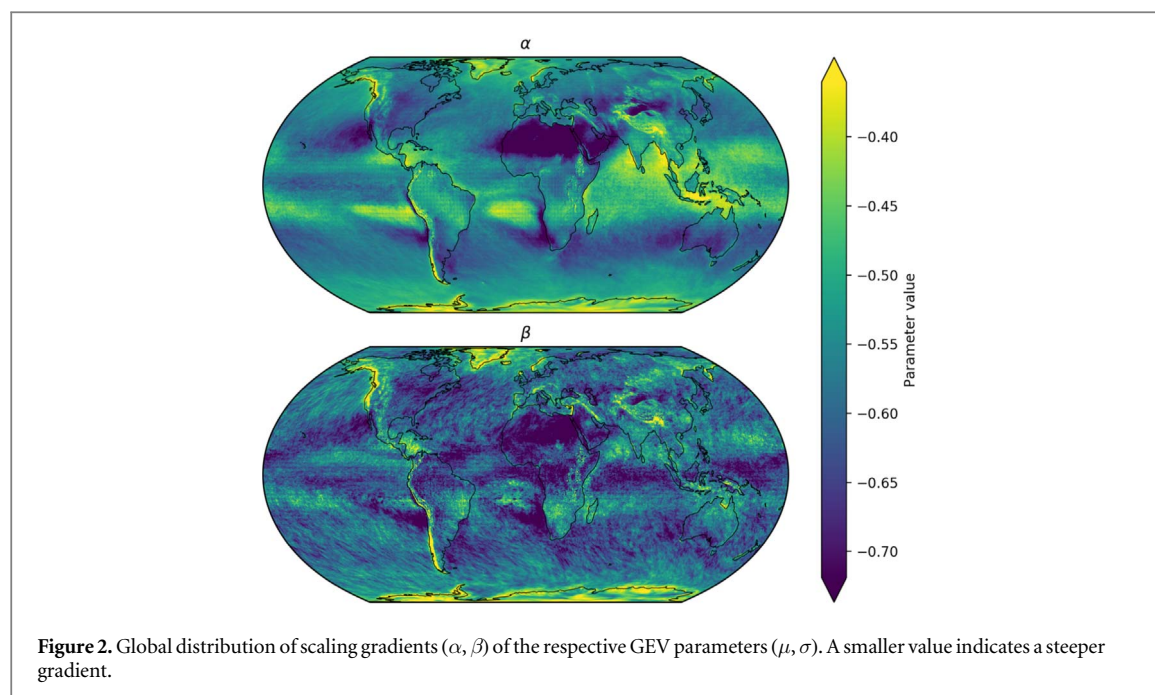
Figure 3 illustrates how this scaling applies for selected global cities. The goodness of fit varies depending on the city, and the fitted regression lines tend to overestimate both GEV parameters at the shortest durations. Additionally, the scale parameter σ displays a weaker linear scaling and higher uncertainty than μ , a property that is in accordance with the r^2 values.

Figure 4 shows the differences between the parameter estimate (PXR-2) and the values derived from the scaling relationship (PXR-4) for both the whole world using ERA5, and at MIDAS rain gauges in the UK (see section 2.1). In the case of the value of the whole world estimated from ERA5 (i.e. the PXR dataset), the application of the scaling relationship induces an overestimation of both μ and σ when $d < 3$ h, of μ when $d > 50$ h, and of σ when $d > 100$ h. When limited to the selected MIDAS gauges the differences for PXR follow the same shape. The differences due to scaling at the MIDAS stations are smaller when using the gauge data, especially for σ , and most notably for $d < 3$ h. Those differences in parameter estimates between PXR-2 and PXR-4 translate to the intensity estimates, with little variation due to the return period (see figure S7).

4. Discussion

4.1. Global GEV parameters

Our analysis (section 3.1, figure S1) concurs with previous work (e.g. Papalexiou and



Koutsoyiannis 2013) suggesting that the AMS of precipitation intensities are usefully described by a GEV distribution. However, using the newly-compiled PXR-2 dataset (Courtney *et al* 2019) we show this applies both on a global scale and with gridded precipitation data.

PXR provides a useful simplified description of global extreme precipitation. By describing the entire intensity–frequency distribution for a given d with only two parameters (i.e. not mean, median, mode, range etc), more meaningful inter-comparison between areas is facilitated, as has been done in other fields in analogous situations (e.g. Hillier *et al* 2013). The utility of PXR is enhanced by the relative ease with which the GEV parameters and their spatial distribution (e.g. figure 1) can be interpreted. Higher μ indicates greater typical precipitation intensities (i.e. the entire distribution becomes more intense), whilst higher σ values indicate more extreme events in the ‘tail’ of the distribution. Additionally, we showed in section 3.1 that the parameter maps constituting PXR-2 represent qualitatively the expected geographical patterns of extreme precipitation, such as monsoon (e.g. south Asia, Kripalani *et al* 2007), mountainous regions (e.g. central Andes, Viale *et al* 2011), or desert areas (e.g. Antarctica, Vaughan *et al* 1999).

This dataset could have many hydrological applications ranging from engineering (e.g. Brown *et al* 2013, NYS DoT 2018) to extreme event studies (e.g. Lumbroso *et al* 2011) and even broader applications such as landslide triggering (e.g. Postance *et al* 2018) or global flood modeling (e.g. Trigg *et al* 2016). Another possible application is as diagnostics for climate and weather models to assess their capacity to reflect the same scalings as those observed in nature.

Our results suggest that μ is broadly more robust than σ . Indeed, the estimates of σ reveal more variability than those of μ in both space (figure 1), duration (figure 3), and the scaling property (figures 2, 4, and S3). This higher variability of σ might be explained by the fact that the scale parameter is related to the intensity of less probable events (i.e. the tail of the probability density function). We acknowledge also that this work employs a relatively short AMS of 40 years that may well miss more extreme events. Indeed, using a longer series of annual maxima is key to improving estimates of GEV parameters (Papalexiou and Koutsoyiannis 2013), although at the risk of overlooking the non-stationary nature of precipitation distributions (Westra *et al* 2014).

Longer AMS could also allow a better estimate of κ . The fixed value of $\kappa = -0.114$ used in this study, based on point rainfall, might not be optimum for areal rainfall and could impact the intensity estimates for long return periods. We acknowledge that the precipitation events considered in this study might not be entirely independent, either in duration or in space, and that the actual confidence interval could be wider than reported here (e.g. Ouarda *et al* 2019, Wilks 2016).

4.2. Scaling in duration of the GEV parameters

Our study confirms that the GEV parameters μ and σ scale robustly with the duration d (e.g. Menabde *et al* 1999, Overeem *et al* 2008), and demonstrate that this relationship applies globally. However, in contrast to previous work there is strong evidence that μ and σ scale with different gradients (see section 3.2). As a caveat, we note that the relationship between the parameters and d may be multi-scale (as denoted by breaks in slope of the log–log plots), and that more

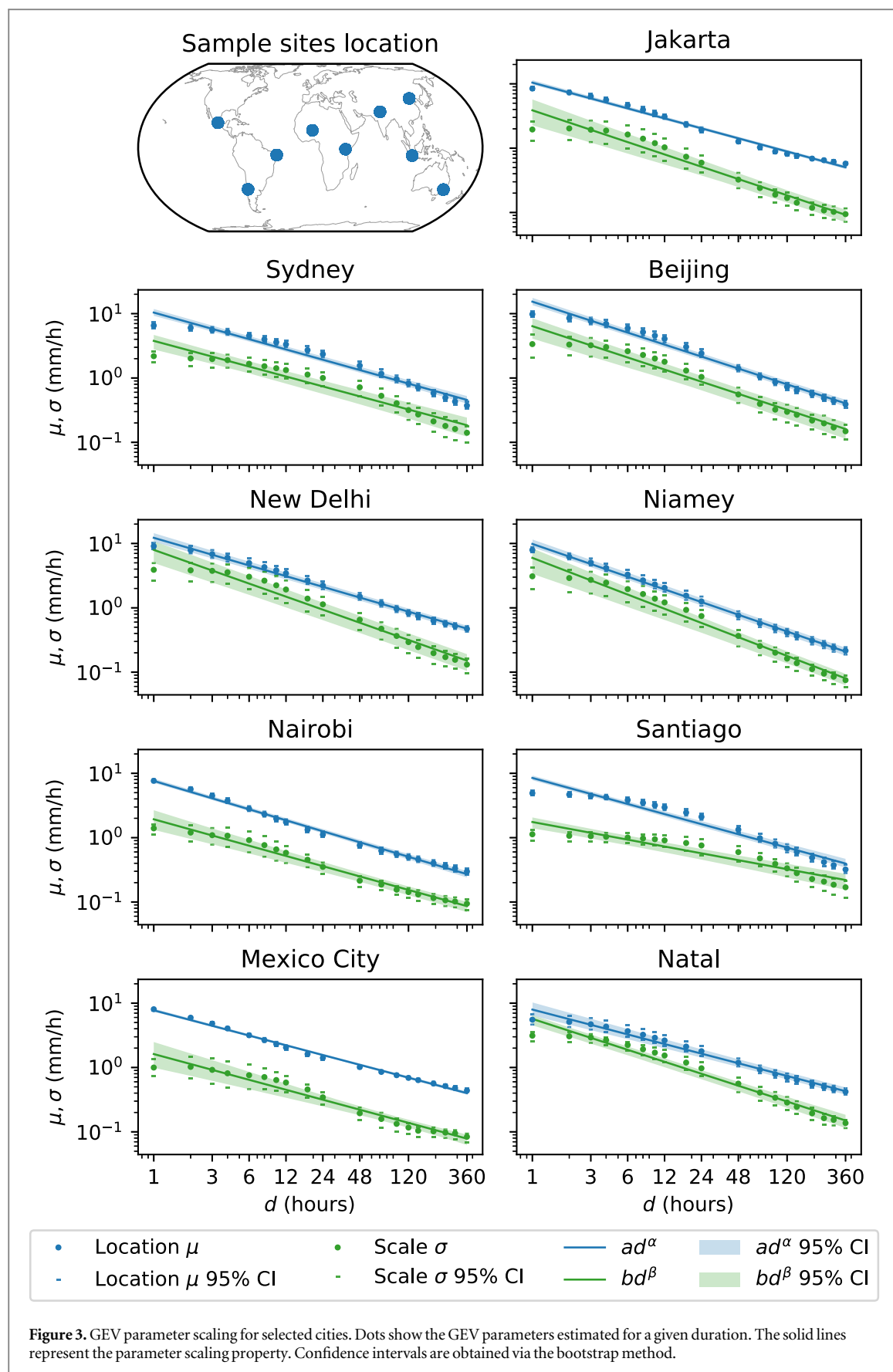
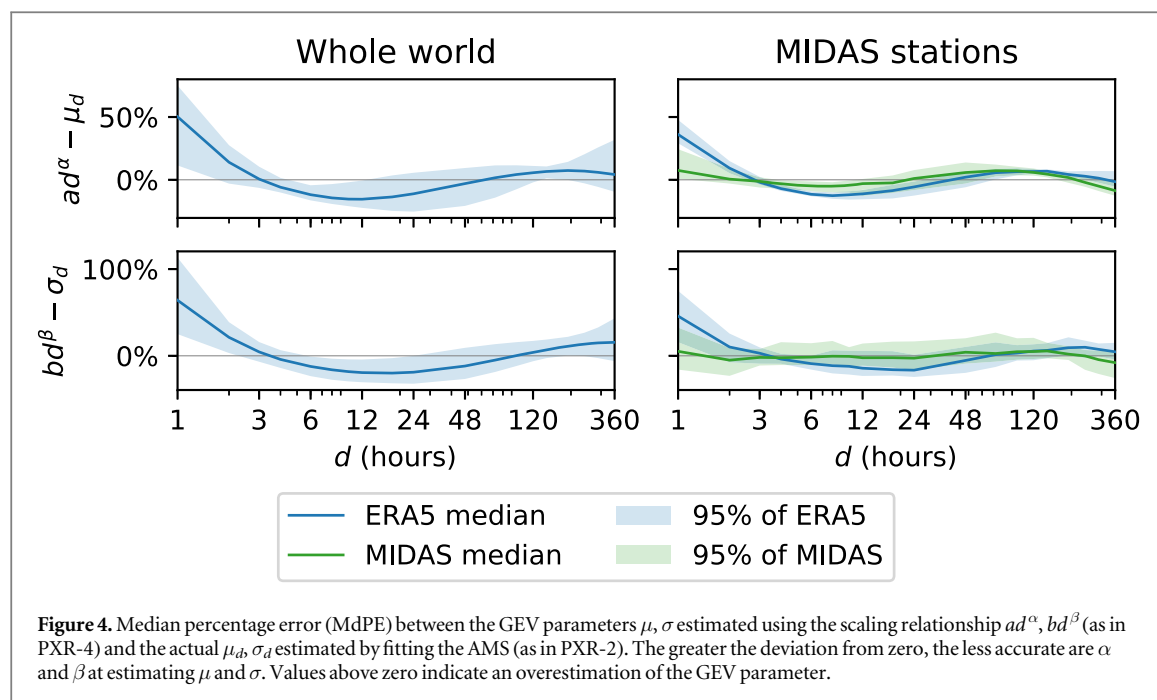


Figure 3. GEV parameter scaling for selected cities. Dots show the GEV parameters estimated for a given duration. The solid lines represent the parameter scaling property. Confidence intervals are obtained via the bootstrap method.

sophisticated scaling laws may be specified (Clauset *et al* 2009). This multi-scaling property has been observed in a similar analysis of radar rainfall (Overeem *et al* 2009), but is not obvious in previous work

using gauges (Menabde *et al* 1999, Overeem *et al* 2008).

We suspect that the scaling differences between ERA5 and the rain gauges (see figure 4) are due to two



main factors. First, the weather model used to generate ERA5 might underestimate the actual precipitation intensities of events of shorter durations, which are likely to be convective in nature and of limited spatial scale (Prein *et al* 2015). This is especially important because the precipitation in ERA5 is modeled, not directly assimilated. Second, the actual scaling property of a gridded product might be inherently different to the scaling of precipitation measured at a point, due to the averaging of rainfall occurring on gridded data. Therefore those differences in scaling might not be due to an inadequacy of the scaling hypothesis, but to an under-reporting of precipitation for events of $d < 3$ h in the ERA5 dataset.

Therefore, in addition to providing sub-daily IDF information in parts of the world where no such data are readily available, PXR-4 also gives an insight about the feasibility of using daily rainfall records from pluviometers to estimate sub-daily IDF. Indeed, daily records are more common than data from automatic sub-daily gauges, and the lack of the latter is a challenge for engineers (e.g. Lumbroso *et al* 2011). Additionally, the parsimonious representation in PXR-4 permits the generation of IDF curves for a continuous range of durations rather than discrete d in the case of PXR-2.

The PXR datasets represent areal precipitation which, as would be expected, results in lower intensities than gauges. For some applications an areal representation is actually preferred, as many hydrological processes of interest take place at the catchment scale. Decades of research have generated insights into the relationship between point and areal rainfall, and the estimation of the areal reduction factor (ARF) (e.g. Rodriguez-Iturbe and Mejia 1974, Asquith and Famiglietti 2000, Kim *et al* 2019). When comparing the

IDF curves from PXR to those created with the MIDAS gauges (see figure 5), we note that the evolution of the median percentage error (MdPE) in both duration and frequency is similar to the expected ARF, with the MdPE decreasing for longer d and shorter T (Pavlovic *et al* 2016).

To illustrate the practical impacts of using PXR-4 or PXR-2, we compare the sizing of a culvert in an hypothetical 80 ha catchment in Jakarta with a time of concentration $T_c = 2$ h. Compared to the use of PXR-2, the use of PXR-4 results in an increase in the catchment outflow by 9.5% for the 10 year rainfall and 14.4% for the 100 year rainfall, which in turn induces a modification in the culvert sizing from 1 to 1.2 m for the 10 year rainfall and 1.2–1.5 m for the 100 year event. In this case, PXR-4 yields a more precautionary and potentially costly design than PXR-2. However, as discussed previously, more research is needed to identify whether those differences are the result of an underestimation of short rainfall intensities from ERA5, or an overestimation due to the scaling law used in PXR-4. For further information on this worked example, see the sizing calculations in section S1.1 and the IDF curves for Jakarta from PXR-2 in figure S8.

5. Concluding remarks

Our results demonstrate the promising applicability of (1) reanalysis data to estimate IDF relationships, and (2) daily rainfall records to estimate sub-daily IDF curves. Our findings may be of notable interest for engineers working in data scarce regions and earth scientists studying extreme precipitation variations. For durations between 2 h and 360 h, the precipitation intensities estimated from PXR-4 are within $\pm 20\%$ of those estimated from PXR-2 (see figure S7).

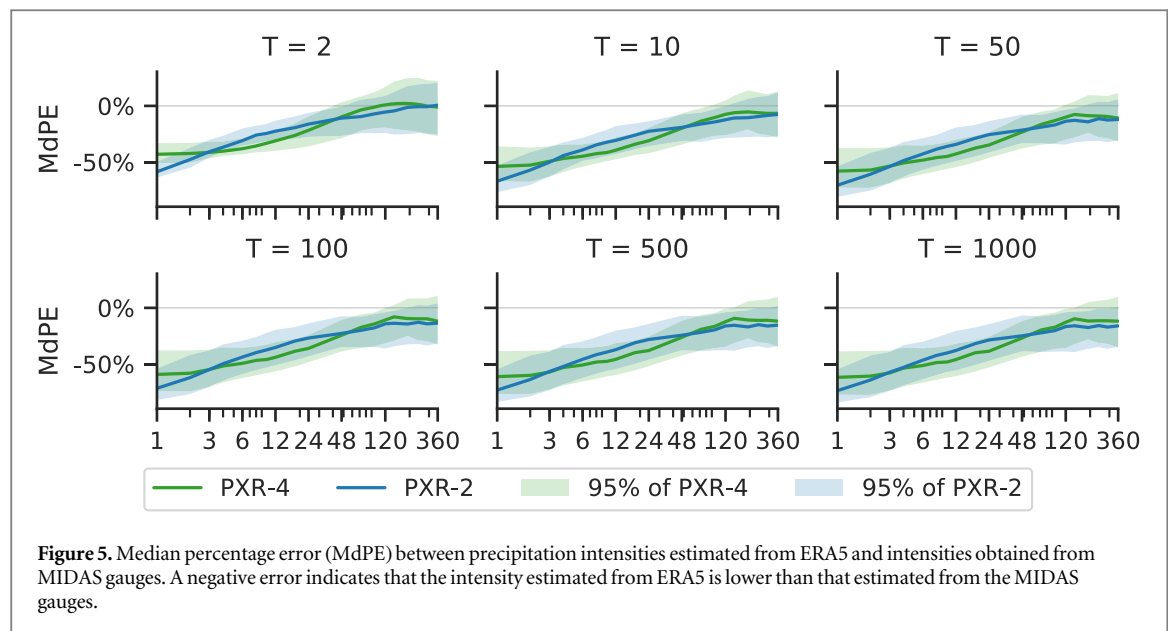


Figure 5. Median percentage error (MdPE) between precipitation intensities estimated from ERA5 and intensities obtained from MIDAS gauges. A negative error indicates that the intensity estimated from ERA5 is lower than that estimated from the MIDAS gauges.

We acknowledge that our research is only a first step in the analysis of global IDF and scaling relationships. More work is needed on the subject, including:

- Studying the range of validity of both PXR-2 and PXR-4 relative to catchment sizes and when compared to other options in data-scarce areas.
- Evaluating the nature of the scaling property, including subhourly precipitation.
- Determining the physical causes of the scaling.
- Comparing the scaling property in both empirical observations and in climate model output.
- Investigating the seasonal variations in the occurrence and scaling of extreme precipitation.
- Evaluating the impact of climate change on the scaling property (e.g. Ouarda *et al* 2019).
- Assessing the use of other probability laws to describe precipitation extremes (e.g. Marani and Ignaccolo 2015, Ouarda *et al* 2019).
- Evaluating the implications of using a fixed κ to fit the GEV, and assessing alternative values or methodologies.
- Studying the impact of precipitation types (snow, hail etc) and processes (orographic, convective etc) on the scaling relationship.
- Examining the underlying factors of the spatial variability observed in both the GEV parameters and their scaling gradients.

In the mean time, PXR-2 and PXR-4 are shared with the research and engineering communities to foster further work on global precipitation extremes.

Acknowledgments

This work is supported by the Natural Environment Research Council (NERC) via grant NE/R014361/1. The results are generated using Copernicus Climate Change Service information 2019. The accompanying PXR-2 and PXR-4 datasets are freely available online (Court *et al* 2019). They include the parameters (μ , σ for PXR-2, a , α , b , β for PXR-4), their confidence intervals and the goodness of fit test values.

The Python programming language was used for the processing and plotting of the data, especially the modules xarray (Hoyer *et al* 2017), dask (Rocklin 2015), pandas (McKinney 2011), Numba (Lam *et al* 2015), matplotlib (Hunter 2007), and Cartopy (Met Office 2010). The software developed for the computation of the results and the creation of the figures is freely available online at <https://github.com/lrntct/pxr>.

The world maps in this paper are drawn using the Equal Earth projection (Šavrič *et al* 2019).

Authors contributions

All authors conceived the research idea, contributed to interpreting the results and writing the manuscript. Laurent Court wrote the software, ran the analysis, and created the figures.

Competing interests

The authors declare no competing interests.

ORCID iDs

Laurent G Court  <https://orcid.org/0000-0002-6241-4802>

Robert L Wilby  <https://orcid.org/0000-0002-4662-9344>
 John K Hillier  <https://orcid.org/0000-0002-0221-8383>
 Louise J Slater  <https://orcid.org/0000-0001-9416-488X>

References

- Ashouri H, Hsu K L, Sorooshian S, Braithwaite D K, Knapp K R, Cecil L D, Nelson B R and Prat O P 2015 PERSIANN-CDR: daily precipitation climate data record from multisatellite observations for hydrological and climate studies *Bull. Am. Meteorol. Soc.* **96** 69–83
- Asquith W and Famiglietti J 2000 Precipitation areal-reduction factor estimation using an annual-maxima centered approach *J. Hydrol.* **230** 55–69
- Battaglia P *et al* 2003 *La Ville et son assainissement Certu ed et al* (Bron: Cerema)
- Beck H E *et al* 2019 Daily evaluation of 26 precipitation datasets using Stage-IV gauge-radar data for the CONUS *Hydrol. Earth Syst. Sci.* **23** 207–24
- Berne A, Delrieu G, Creutin J D and Obled C 2004 Temporal and spatial resolution of rainfall measurements required for urban hydrology *J. Hydrol.* **299** 166–79
- Bland J M and Altman D G 1995 Multiple significance tests: the Bonferroni method *BMJ (Clinical Research Ed)* **310** 170
- Blenkinsop S *et al* 2018 The INTENSE project: using observations and models to understand the past, present and future of sub-daily rainfall extremes *Adv. Sci. Res.* **15** 117–26
- Blenkinsop S, Lewis E, Chan S C and Fowler H J 2017 Quality-control of an hourly rainfall dataset and climatology of extremes for the UK *Int. J. Climatol.* **37** 722–40
- Bougadis J and Adamows K 2006 Scaling model of a rainfall intensity-duration-frequency relationship *Hydrol. Process.* **20** 3747–57
- Brown S A, Schall J D, Morris J L, Doherty C L, Stein S M and Warner C C 2013 *Urban Drainage Design Manual* vol 2009 3rd edn (Arlington, VA: National Highway Institute)
- Chow V T 1959 *Open Channel Hydraulics* (New York: McGraw-Hill)
- Clauset A, Shalizi C R and Newman M E J 2009 Power-law distributions in empirical data *SIAM Rev.* **51** 661–703
- Copernicus Climate Change Service 2018 Climate Data Store (<https://cds.climate.copernicus.eu>)
- Courty L G, Wilby R L, Hillier J K and Slater L J 2019 Parametrized eXtreme Rain (<https://zenodo.org/record/2616438#.XU6tW2R7mUk>)
- Domínguez R, Carrizosa E, Fuentes G E, Arganis M L, Osnaya J and Galván-Torres A E 2018 Análisis regional para estimar precipitaciones de diseño en la república mexicana *Tecnol. Cienc. Agua* **9** 05–29
- Fowler H J and Kilsby C G 2003 A regional frequency analysis of United Kingdom extreme rainfall from 1961 to 2000 *Int. J. Climatol.* **23** 1313–34
- Gelaro R *et al* 2017 The modern-era retrospective analysis for research and applications, version 2 (MERRA-2) *J. Clim.* **30** 5419–54
- Hao Z, AghaKouchak A, Nakhjiri N and Farahmand A 2014 Global integrated drought monitoring and prediction system *Sci. Data* **1** 140001
- Heo J H, Kho Y W, Shin H, Kim S and Kim T 2008 Regression equations of probability plot correlation coefficient test statistics from several probability distributions *J. Hydrol.* **355** 1–15
- Hersbach H and Dick L 2016 ERA5 reanalysis is in production *ECMWF Newsletter* 147 p 7 (<http://ecmwf.int/sites/default/files/elibrary/2016/16299-newsletter-no147-spring-2016.pdf>)
- Hillier J, Smith M, Clark C, Stokes C and Spagnolo M 2013 Subglacial bedforms reveal an exponential size-frequency distribution *Geomorphology* **190** 82–91
- Hosking J R M, Wallis J R and Wood E F 1985 Estimation of the generalized extreme-value distribution by the method of probability-weighted moments *Technometrics* **27** 251–61
- Hoyer S and Hamman J 2017 Xarray: N-D labeled arrays and datasets in python *J. Open Res. Softw.* **5** 10 (<http://openresearchsoftware.metajnl.com/articles/10.5334/jors.148/>)
- Hunter J D 2007 Matplotlib: a 2D graphics environment *Comput. Sci. Eng.* **9** 90–5
- Kim J, Lee J, Kim D and Kang B 2019 The role of rainfall spatial variability in estimating areal reduction factors *J. Hydrol.* **568** 416–26
- Koutsoyiannis D 2004a Statistics of extremes and estimation of extreme rainfall: I. Theoretical investigation/Statistiques de valeurs extrêmes et estimation de précipitations extrêmes: I. Recherche théorique *Hydrol. Sci. J.* **49** 590 (<https://tandfonline.com/doi/full/10.1623/hysj.49.4.575.54430>)
- Koutsoyiannis D 2004b Statistics of extremes and estimation of extreme rainfall: II. Empirical investigation of long rainfall records *Hydrol. Sci. J.* **49** 610 (<https://tandfonline.com/doi/full/10.1623/hysj.49.4.575.54430>)
- Kripalani R H, Oh J H, Kulkarni A, Sabade S S and Chaudhari H S 2007 South Asian summer monsoon precipitation variability: coupled climate model simulations and projections under IPCC AR4 *Theor. Appl. Climatol.* **90** 133–59
- Kumari M, Singh C K and Basistha A 2017 Clustering data and incorporating topographical variables for improving spatial interpolation of rainfall in mountainous region *Water Resour. Manage.* **31** 425–42
- Lam S K, Pitrou A and Seibert S 2015 Numba: a LLVM-based Python JIT compiler *Proc. 2nd Workshop on the LLVM Compiler Infrastructure in HPC—LLVM '15* (New York: ACM) pp 1–6
- Lu L H and Stedinger J R 1992 Variance of two- and three-parameter GEV/PWM quantile estimators: formulae, confidence intervals, and a comparison *J. Hydrol.* **138** 247–67
- Lumbroso D, Boyce S, Bast H and Walmsley N 2011 The challenges of developing rainfall intensity-duration-frequency curves and national flood hazard maps for the Caribbean *J. Flood Risk Manage.* **4** 42–52
- Marani M and Ignaccolo M 2015 A metastatistical approach to rainfall extremes *Adv. Water Res.* **79** 121–6
- McKinney W 2011 Pandas: a foundational python library for data analysis and statistics *Proc. 1st Workshop on Python for High-Performance and Scientific Computing*
- Menabde M, Seed A and Pegram G 1999 A simple scaling model for extreme rainfall *Water Resour. Res.* **35** 335–9
- Met Office 2010 Cartopy (<https://scitools.org.uk/cartopy>)
- Met Office 2012 Met Office Integrated Data Archive System (MIDAS) Land and Marine Surface Stations Data (1853-current), (<http://catalogue.ceda.ac.uk/uuid/220a65615218d5c9cc9e4785a3234bd0>)
- Met Office 2018 UK Climate—Extremes (<https://web.archive.org/web/20181206185424/https://www.metoffice.gov.uk/public/weather/climate-extremes/>)
- NYS DoEC 1989 Guidelines for design of dams *Technical Report* New York State Department of Environmental Conservation
- NYS DoT 2018 Highway drainage *Highway Design Manual* New York State Department of Transportation (<https://dot.ny.gov/divisions/engineering/design/dqab/hdm/chapter-8>)
- Olauson J 2018 ERA5: the new champion of wind power modelling? *Renew. Energy* **126** 322–31
- Ombadi M, Nguyen P, Sorooshian S and Hsu K I 2018 Developing intensity-duration-frequency (IDF) curves from satellite-based precipitation: methodology and evaluation *Water Resour. Res.* **54** 7752–66
- Ouarda T B M J, Yousef L A and Charron C 2019 Non stationary intensity duration frequency curves integrating information concerning teleconnections and climate change *Int. J. Climatol.* **39** 2306–23
- Overeem A, Buishand A and Holleman I 2008 Rainfall depth-duration-frequency curves and their uncertainties *J. Hydrol.* **348** 124–34

- Overeem A, Buishand T A and Holleman I 2009 Extreme rainfall analysis and estimation of depth-duration-frequency curves using weather radar *Water Resour. Res.* **45** 1–15
- Papalexiou S M and Koutsoyiannis D 2013 Battle of extreme value distributions: a global survey on extreme daily rainfall *Water Resour. Res.* **49** 187–201
- Pavlovic S, Perica S, Laurent M St and Mejia A 2016 Intercomparison of selected fixed-area areal reduction factor methods *J. Hydrol.* **537** 419–30
- Postance B, Hillier J, Dijkstra T and Dixon N 2018 Comparing threshold definition techniques for rainfall-induced landslides: a national assessment using radar rainfall *Earth Surf. Process. Landf.* **43** 553–60
- Prein A F *et al* 2015 A review on regional convection-permitting climate modeling: demonstrations, prospects, and challenges *Rev. Geophys.* **53** 323–61
- Ragulina G and Reitan T 2017 Generalized extreme value shape parameter and its nature for extreme precipitation using long time series and the Bayesian approach *Hydrol. Sci. J.* **62** 863–79
- Rocklin M 2015 Dask: parallel computation with blocked algorithms and task scheduling *Proc. 14th Python in Science Conf.* ed K Huff and J Bergstra pp 130–6
- Rodriguez-Iturbe I and Mejia J M 1974 On the transformation of point rainfall to areal rainfall *Water Resour. Res.* **10** 729–35
- Roux C and Desbordes M 1996 Rainfall-frequency curves with a recent urban dense rainfall measurement network *Atmos. Res.* **42** 163–76
- Šavrič B, Patterson T and Jenny B 2019 The equal Earth map projection *Int. J. Geogr. Inf. Sci.* **33** 454–65
- Staffell I and Pfenninger S 2016 Using bias-corrected reanalysis to simulate current and future wind power output *Energy* **114** 1224–39
- Sun Q, Miao C, Duan Q, Ashouri H, Sorooshian S and Hsu K L 2018 A review of global precipitation data sets: data sources, estimation, and intercomparisons *Rev. Geophys.* **56** 79–107
- Texas Department of Transportation 2016 *Hydraulic Design Manual* Texas Department of Transportation
- Trigg M A *et al* 2016 The credibility challenge for global fluvial flood risk analysis *Environ. Res. Lett.* **11** 094014
- UN DESA 2018 Revision of world urbanization prospects *Technical Report* United Nations (<https://un.org/development/desa/publications/2018-revision-of-world-urbanization-prospects.html>)
- Uppala S M *et al* 2005 The ERA-40 re-analysis *Q. J. R. Meteorol. Soc.* **131** 2961–3012
- van de Giesen N, Hut R and Selker J 2014 The trans-african hydro-meteorological observatory (TAHMO) *Wiley Interdiscip. Rev.: Water* **1** 341–8
- Vaughan D G, Bamber J L, Giovinetto M, Russell J, Cooper A P R, Vaughan D G, Bamber J L, Giovinetto M, Russell J and Cooper A P R 1999 Reassessment of net surface mass balance in antarctica *J. Clim.* **12** 933–46
- Veneziano D and Furcolo P 2002 Multifractality of rainfall and scaling of intensity-duration-frequency curves *Water Resour. Res.* **38** 42-1
- Viale M, Nuñez M N, Viale M and Nuñez M N 2011 Climatology of winter orographic precipitation over the subtropical central andes and associated synoptic and regional characteristics *J. Hydrometeorol.* **12** 481–507
- Westra S, Fowler H J, Evans J P, Alexander L V, Berg P, Johnson F, Kendon E J, Lenderink G and Roberts N M 2014 Future changes to the intensity and frequency of short-duration extreme rainfall *Rev. Geophys.* **52** 522–55
- Wilks D 2011 Frequentist statistical inference *Int. Geophys.* **100** 133–86
- Wilks D S 2016 The stippling shows statistically significant grid points: how research results are routinely overstated and overinterpreted, and what to do about it *Bull. Am. Meteorol. Soc.* **97** 2263–73
- Xu W, Zou Y, Zhang G and Linderman M 2015 A comparison among spatial interpolation techniques for daily rainfall data in Sichuan Province, China *Int. J. Climatol.* **35** 2898–907